Optics Communications 283 (2010) 4342–4345

Contents lists available at ScienceDirect

Optics Communications

journal homepage: www.elsevier.com/locate/optcom

Bi-directional spatial soliton emission at engineered nonlinear waveguide interfaces

Fabio Baronio [a,*], Costantino De Angelis [a], Vincent Couderc [b], Alain Barthélémy [b], Wolfgang Sohler [c]

[a] CNISM and Università di Brescia, Via Branze 38, 25123 Brescia, Italy
[b] XLIM, CNRS and Université de Limoges, Av. Albert Thomas 123, 87060, Limoges, France
[c] Angewandte Physik, Universitat Paderborn, 33095 Paderborn, Germany

ARTICLE INFO

Article history:
Received 29 April 2010
Received in revised form 7 June 2010
Accepted 7 June 2010

Keywords:
Solitons
Quasi-phase-matching
Second harmonic generation

ABSTRACT

We observed tunable bi-directional emission of spatial solitons at a quadratically nonlinear interface in periodically poled lithium niobate planar waveguides. The interface consists of the boundary between two quasi-phase-matched regions with a different poling period. We show the intensity and phase-mismatch (temperature or wavelength) dependence of the phenomena.

1. Introduction

Self-localized light packets in space or spatial solitary waves have attracted a great deal of attention in both fundamental and applied scenarios, owing to their potentials in novel generations of fully reconfigurable self-sustained photonic circuits. They have been observed and investigated in various nonlinear systems including quadratic, cubic, photovoltaic, photorefractive, reorientational and dissipative media [1–8]. An interesting aspect that has received little attention is the propagation of solitons in finite-size media, particularly in the case of a nonlocal response, where the proximity to an interface can have effects on the trajectory of a soliton. The latter aspect has been addressed theoretically [9–15] and experimentally [16–22] for a few nonlinearities, including Kerr, saturable, quadratic, photorefractive, thermo-optic, and reorientational.

In the framework of quadratic nonlinear media, the quasi-phase-matching technique can be exploited to produce engineered nonlinear structures. This opens a whole range of new possibilities experimentally feasible with the progress of a reproducible fabrication of periodically poled $LiNbO_3$ (PPLN) and KTP (PPKTP) [23,24]. Quadratic soliton reflection at a planar interface separating two shifted PPKTP regions with the same poling patterns [17] and at a planar interface separating PPLN and $LiNbO_3$ regions [18] were observed. Moreover, unidirectional spatial soliton emission at the planar interface separating PPLN and $LiNbO_3$ regions was demonstrated [25].

In this article, we report for the first time the observation of a temperature (wavelength) tunable bi-directional spatial soliton emission at a planar interface separating PPLN regions with different poling patterns. This PPLN boundary exhibits a temperature and/or wavelength dependent tunable repulsive potential when powerful optical beams propagate in its vicinity. Self-induced reorientation of the incident beam is predicted [13].

We refer to electromagnetic nonlinear type I interaction of a fundamental wave [(FF) at 1548 nm] and a second harmonic wave [(SH) at 774 nm]. We describe the spatial dynamics of beams that propagate across a quadratically nonlinear interface in titanium-indiffused periodically poled lithium niobate slab waveguides. The interface consists of the boundary between two quasi-phase-matched regions with different poling periods. Only the FF wave was launched into the waveguide (see Fig. 1). In the whole device the linear refractive index is homogeneous. In this situation, in the low-intensity linear regime the beam propagates along the interface without changing its trajectory. In the high-intensity nonlinear regime, depending on the temperature or wavelength (i.e., phase-mismatch conditions) we observed left or right spatial soliton emission. In the emission regime the beam propagates along the interface, it creates a nonlinear potential barrier leading to spatial self-refraction.

2. Experimental set-up and theoretical model

The experiments were performed in a 70 mm long Ti:$LiNbO_3$ planar waveguide fabricated in a Z-cut substrate by indiffusion of a 70 nm thick, vacuum-deposited Ti-layer at 1064 °C during 9 h. Two transversely interfaced micro-domain structures of 16.67 μm (P1) and of 16.74 μm (P2) periodicity, designed for frequency doubling at 1548 nm, were generated after waveguide fabrication by electric field assisted poling. Thus, the sample exhibited a transition (the nonlinear phase-mismatched interface) between two periodically poled regions of different periodicities (see Fig. 1). The sample was inserted in a temperature stabilized oven to allow operation at elevated temperatures (phase-matching SH generation occurred at $T = 216$ °C in P1 and at $T = 198$ °C in

* Corresponding author.
E-mail address: baronio@ing.unibs.it (F. Baronio).

0030-4018/$ – see front matter © 2010 Elsevier B.V. All rights reserved.
doi:10.1016/j.optcom.2010.06.029

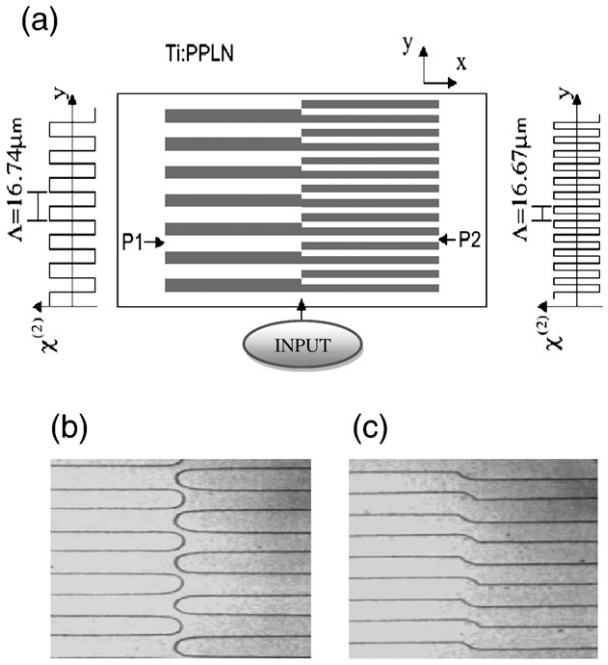

Fig. 1. (a) Schematic top view of the nonlinear engineered interface; (b), (c) photographs of a section of the engineered Ti:PPLN waveguide surface with the phase-mismatched nonlinear interface.

P2); in this way, photorefractive effects ('optical damage') could be minimized. Moreover, temperature-tuning of the phase-matching conditions became possible. An all-fiber laser system was used as the source of 5 ps pulses (FWHM in intensity) at 1548 nm (FF) of 1.7 nm spectral bandwidth and of a peak power of a few kilowatts at 20 MHz repetition rate. The waveguide was designed in such a way that single mode propagation (TM_0) was guaranteed at the FF; several TM modes are supported at the second harmonic (SH), but only the TM_0 mode of 3 μm FWHM is efficiently generated by the TM_0 at the FF. The laser beam was shaped in a highly elliptical spot, nearly gaussian in profile, with a spot of 4 μm (FWHM in intensity) along the guided dimension (z direction) and with a spot of 80 μm along the perpendicular direction (x), and was polarized parallel to the Z axis of the PPLN to take advantage of the material's largest quadratic nonlinear coefficient $\chi^{(2)}_{zzz}=2d_{33}=54$ pm/V. The spatial beam profiles were recorded by imaging the output pattern on a vidicon camera. Temporal characterizations were monitored by a background free non-collinear auto-correlator. Two different filters were alternatively introduced, to select either the IR-FF or the SH output.

We model the electric fields E_1 and E_2, at ω_0 (FF) and $2\omega_0$ (SH) respectively, with $\omega_0=2\pi/\lambda_0$ and $\lambda_0=1548$ nm free space wavelength, propagating in the y direction, as $E_1(x,y,z,t)=1/2[m_1(z)a_1(x,y,t)\exp(-j(\beta_{\omega_0}y+\omega_0 t))+c.c.]$ and $E_2(x,y,z,t)=1/2[m_2(z)a_2(x,y,t)\exp(-j(\beta_{2\omega_0}y+2\omega_0 t))+c.c.]$; $m_1(z)$ and $m_2(z)$ are the mode profiles in the guided dimension, $a_1(x,y,t)$ and $a_2(x,y,t)$ are the slowly varying envelopes, that obey the nonlinear coupled equations:

$$
\begin{aligned}
&i\frac{\partial a_1}{\partial y}-i\beta'_{\omega_0}\frac{\partial a_1}{\partial t}-\frac{\beta''_{\omega_0}}{2}\frac{\partial^2 a_1}{\partial t^2}+\frac{1}{2\beta_{\omega_0}}\frac{\partial^2 a_1}{\partial x^2}+\\
&\quad+\frac{\chi^{(2)}\omega_0}{2cn_{\omega_0}}\frac{\int m_2|m_1|^2dz}{\int|m_1|^2dz}a_2a_1^*e^{-j\Delta k(x)y}=0,\\
&i\frac{\partial a_2}{\partial y}-i\beta'_{2\omega_0}\frac{\partial a_2}{\partial t}-\frac{\beta''_{2\omega_0}}{2}\frac{\partial^2 a_2}{\partial t^2}+\frac{1}{2\beta_{2\omega_0}}\frac{\partial^2 a_2}{\partial x^2}+\\
&\quad+\frac{\chi^{(2)}\omega_0}{2cn_{2\omega_0}}\frac{\int m_2|m_1|^2dz}{\int|m_2|^2dz}a_1^2e^{j\Delta k(x)y}=0,
\end{aligned}
\tag{1}
$$

where β represents the propagation constant, β' the inverse group velocity, β'' the inverse group-velocity dispersion; n is the refractive index, $\Delta k(x)=2\beta_{\omega_0}-\beta_{2\omega_0}+K_S(x)$ is the effective mismatch, where $K_S(x)=2\pi/\Lambda(x)$ and $\chi^{(2)}=(2/\pi)\chi^{(2)}_{zzz}$ is the nonlinear coefficient. We assumed that the nonlinear interface is located at $x=0$ in the (y,z) plane. To model the pulse propagation, two different numerical tools have been used. A standard finite difference vectorial mode solver was employed to determine the linear propagation properties in the slab waveguide, i.e. the mode profiles, the effective index, the propagation constant, the inverse group velocity and the inverse group-velocity dispersion. In the case at hand: $\beta_{\omega_0}=8.69\cdot10^6\,[\mathrm{m}^{-1}]$, $\beta_{2\omega_0}=17.8\cdot10^6\,[\mathrm{m}^{-1}]$, $\beta'_{\omega_0}=7.29\cdot10^{-9}$[s/m], $\beta'_{2\omega_0}=7.656\cdot10^{-9}$[s/m], $\beta''_{\omega_0}=1.18\cdot10^{-25}\,[\mathrm{s}^2/\mathrm{m}]$, $\beta''_{2\omega_0}=4.1\cdot10^{-25}\,[\mathrm{s}^2/\mathrm{m}]$, $\chi^{(2)}_{zzz}=54$[pm/V]. Moreover $\frac{\chi^{(2)}\omega_0}{2cn_{\omega_0}}\frac{\int m_2|m_1|^2dy}{\int|m_1|^2dy}=\frac{\chi^{(2)}\omega_0}{2cn_{2\omega_0}}\frac{\int m_2|m_1|^2dy}{\int|m_2|^2dy}=0.1944\left[\Omega^{\frac{1}{2}}V^{-1}m^{-\frac{1}{2}}\right]$, normalizing $\frac{1}{2\eta_{\omega_0}}\int|m_1|^2dy=1$ and $\frac{1}{2\eta_{2\omega_0}}\int|m_2|^2dy=1$. The power is represented by $P(z,t)=\int|a_1(x,z,t)|^2dx+\int|a_2(x,z,t)|^2dx$[W]. The crystal length corresponds to 3.7 times the FF diffraction length and to 5.6 times the walk-off length between FF and SH;

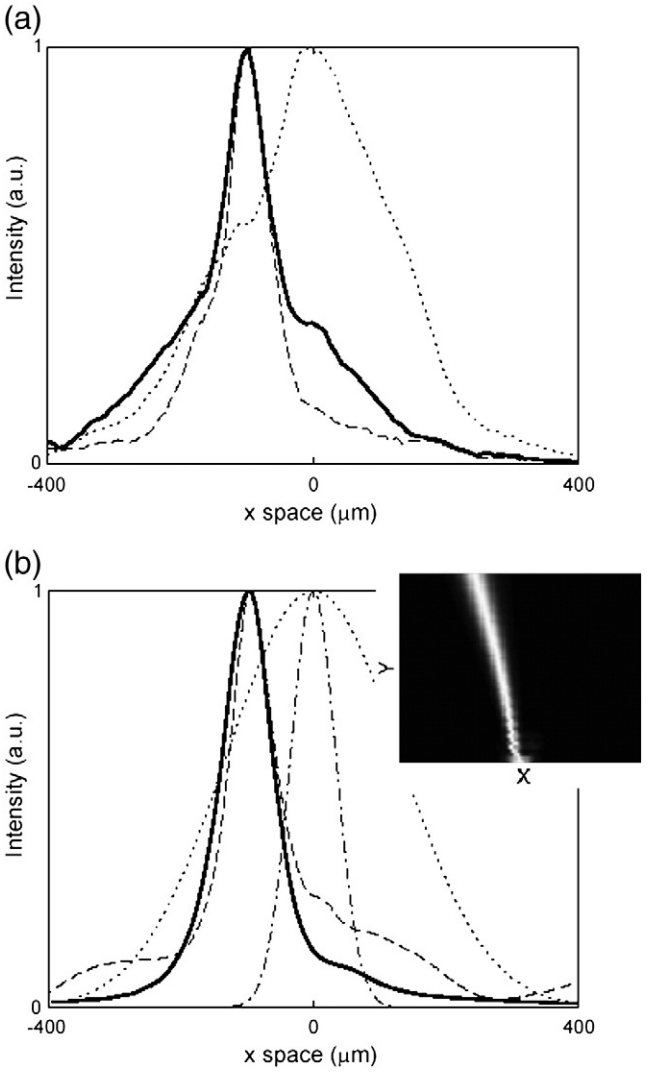

Fig. 2. (a) Measured and (b), calculated spatial output profiles, taken at $T=204$°C: FF beam in linear regime (dotted curve); FF beam (solid curve) and SH beam (dashed curve) at $I=160$ MW/cm^2. The dash–dotted curve in (b) represents the FF input profile. The inset shows the numerical FF spatial evolution in the (x,y) plane, at $I=160$ MW/cm^2 (x[−400 μm, 400 μm], y[0,70 mm]).

the dispersive terms can be neglected. The phase-mismatch temperature dependency corresponds approximately to $1.66\pi/°C$. The phase-mismatch jump at the nonlinear interface is about $30\pi(\Delta kL)$. Finally, using a finite difference beam propagation technique, we solved the nonlinear coupled Eq. 1.

3. Bi-directional soliton emission

We carried out experiments and numerical simulations by launching a FF input beam parallel to the nonlinear interface (see Fig. 1a), varying the phase-mismatch conditions by the temperature of the sample, and the input pulse power, keeping fixed the temporal and spatial widths of the injected FF pulse.

At first, we fixed the temperature T at 204 °C. In this situation, the phase-mismatch conditions in the two uniform regions are $\Delta kL_{P1} = 20\pi$ and $\Delta kL_{P2} = -10\pi$. In the quasi-linear regime, at low intensity, the beam broadened because of diffraction inside the crystal. By increasing the incident intensity, in the nonlinear regime, we succeeded in exciting a spatial soliton and we observed its spatial emission. In Fig. 2, typical numerical and experimental results are shown. The beam experienced an intensity dependent effective spatial acceleration and consequently spatial velocity in the transverse dimension (x) towards the P1 region. The soliton formation distance is about 10 mm. The lateral velocity undergone by the self trapped beam increases with the input intensity. In Fig. 3, typical numerical and experimental results are shown.

In a second step, we fixed the temperature T at 185 °C. In this condition, the new phase-mismatch conditions are positive in both regions and are equal to: $\Delta kL_{P1} = 51\pi$ and $\Delta kL_{P1} = 21\pi$. Again, in the quasi-linear regime, at low intensity, the beam broadened because of diffraction inside the crystal. By increasing the incident intensity, in the nonlinear regime, we succeeded in exciting a single spatial soliton and we observed its spatial emission. The beam experienced an intensity dependent effective spatial acceleration and consequently spatial velocity in the transverse dimension (x) but with opposite direction compared to the first experiment. Because of the positive/positive phase-mismatch conditions, the potential due to the nonlinear interface repulses the soliton beam toward the region which exhibits the better nonlinear efficiency (P2 region). In Fig. 4, typical numerical and experimental results are shown.

The phenomenon of nonlinear soliton emission can be attributed to the existence of a nonlinear potential barrier. In the limit of large

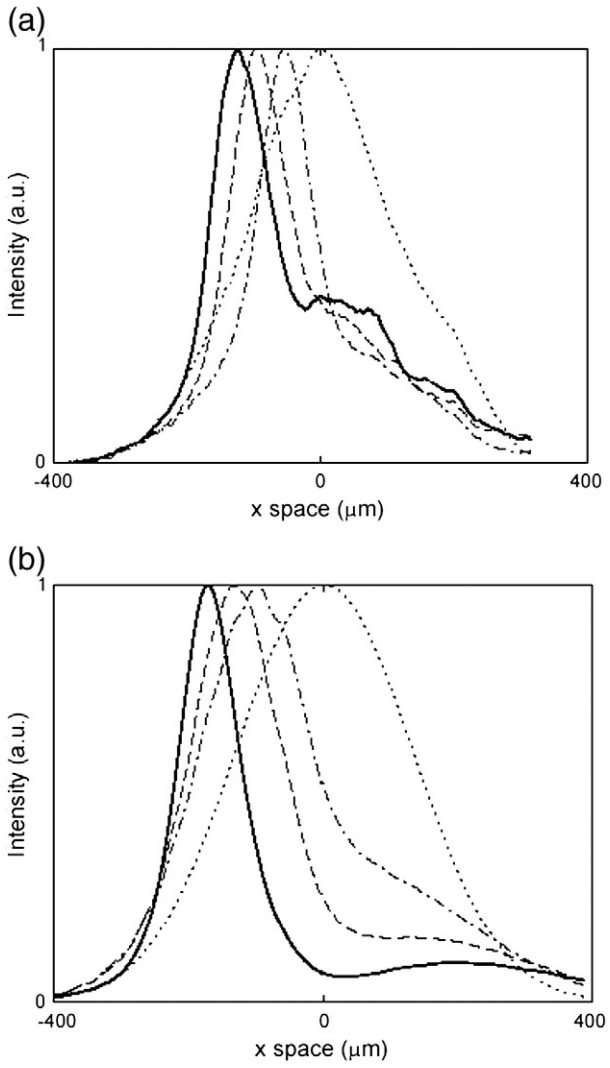

Fig. 3. (a) Measured and (b), calculated FF spatial output profiles, taken at $T = 204$ °C, at different input intensities: $I = 1$ MW/cm^2 (dotted curve, quasi-linear regime); $I = 70$ MW/cm^2 (dash–dotted); $I = 120$ MW/cm^2 (dashed curve); $I = 180$ MW/cm^2 (solid curve).

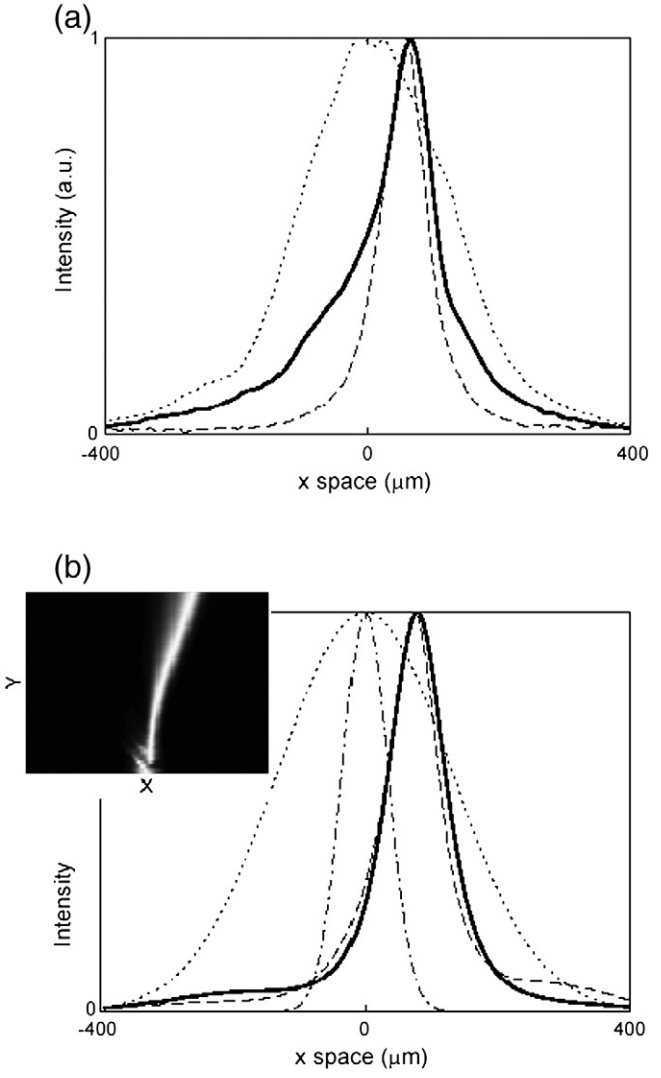

Fig. 4. (a) Measured and (b), calculated spatial output profiles, taken at $T = 185$ °C: FF beam in linear regime (dotted curve); FF beam (solid curve) and SH beam (dashed curve) at $I = 160$ MW/cm^2. The dash–dotted curve in (b) represents the FF input profile. The inset shows the numerical FF spatial evolution in the (x,y) plane, at $I = 160$ MW/cm^2 (x[−400 μm, 400 μm], y[0,70 mm]).

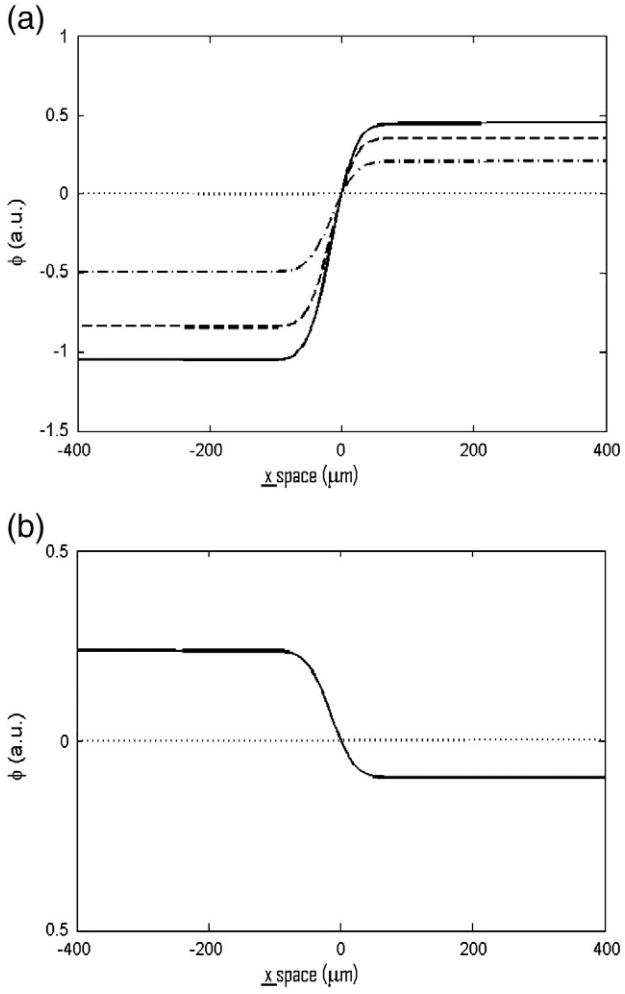

Fig. 5. (a) $T=204$ °C. Effective induced potential for various beam intensities: $I=1$ MW/cm^2 (dotted curve, quasi-linear regime); $I=70$ MW/cm^2 (dash–dotted); $I=120$ MW/cm^2 (dashed curve); $I=180$ MW/cm^2 (solid curve). (b) $T=180$ °C. Effective induced potential at $I=1$ MW/cm^2 (dotted curve, quasi-linear regime) and $I=160$ MW/cm^2 (solid curve).

phase-mismatch, an equation of motion for the FF field can be derived from Eq. (1) [26]:

$$i\frac{\partial a_1}{\partial y}-i\beta'_{\omega_0}\frac{\partial a_1}{\partial t}-i\frac{\beta''_{\omega_0}}{2}\frac{\partial^2 a_1}{\partial t^2}+\frac{1}{2\beta_{\omega_0}}\frac{\partial^2 a_1}{\partial x^2}+\frac{\chi_{FF}\chi_{SH}}{\Delta k(x)}|a_1|^2a_1+ -2j\delta\frac{\chi_{FF}\chi_{SH}}{\Delta k(x)^2}|a_1|^2\frac{\partial a_1}{\partial t}=0 \quad (2)$$

where

$$\chi_{FF}=\frac{\chi^{(2)}\omega_0}{2cn_{\omega_0}}\frac{\int m_2|m_1|^2dz}{\int|m_1|^2dz},\quad \chi_{SH}=\frac{\chi^{(2)}\omega_0}{2cn_{2\omega_0}}\frac{\int m_2|m_1|^2dz}{\int|m_2|^2dz}. \quad (3)$$

Analyzing the FF beam dynamics by the effective-particle model for the motion of $\underline{x}$, the average position in the x direction [11], yields

$$\frac{d^2\underline{x}}{dz^2}=\frac{\int\frac{dF}{d\underline{x}}|a_1|^2dx}{\int|a_1|^2dx}=-\frac{d\phi(\underline{x})}{d\underline{x}},\quad F=\frac{\chi_{FF}\chi_{SH}}{\Delta k(x)}|a_1|^2. \quad (4)$$

F represents the nonlinear refractive index, which does not depend on the steepening term (because the steepening term, being symmetric in x, does not affect the beam trajectory). $\phi(\underline{x})$ is the effective potential that the effective particle feels. The effective potential determining the dynamics of the beams in Figs. 3 and 4 are shown in Fig. 5. The properties of the nonlinear barrier are phase-mismatch dependent (temperature or wavelength) and intensity dependent. The phase-mismatched interface does not affect low-amplitude waves. These phenomena are genuine quadratic soliton features.

4. Conclusions

In conclusion, we have observed bi-directional spatial emission of picosecond signals at 1549 nm at an engineered quadratically nonlinear interface in periodically poled lithium niobate planar waveguides. We show the intensity and phase-mismatch dependence of the phenomena. These observations make possible several soliton processing schemes, including a power-controlled steering and/or a wavelength-controlled (phase-mismatched controlled) steering.

References

[1] Y. Kivshar, G. Agrawal, Academic (2003).
[2] S. Trillo, W. Torruellas (Eds.), Spatial Solitons, Springer-Verlag, Berlin, 2001.
[3] G. Stegeman, M. Segev, Science 286 (1999) 1518.
[4] M. Peccianti, C. Conti, G. Assanto, A. De Luca, C. Umeton, Nature 432 (2004) 733.
[5] C. Conti, A. Fratalocchi, M. Peccianti, G. Ruocco, S. Trillo, Phys. Rev. Lett. 102 (2009) 083902.
[6] A. Pasquazi, G. Assanto, Phys. Rev. A 80 (2009) 021801.
[7] N. Akhmediev, A. Ankiewicz, J. Soto-Crespo, P. Grelu, IJBC 19 (2009) 2621.
[8] F. Baronio, M. Conforti, C. De Angelis, A. Degasperis, M. Andreana, V. Couderc, A. Barthelemy, Phys. Rev. Lett. 104 (2010) 113902.
[9] A. Aceves, J. Moloney, A. Newell, Phys. Rev. A 39 (1989) 1809.
[10] Y. Kivshar, A. Kosevich, O. Chubykalo, Phys. Rev. A 41 (1990) 1677.
[11] A. Capobianco, C. De Angelis, A. Laureti Palma, G. Nalesso, J. Opt. Soc. Am. B 14 (1997) 1956.
[12] J. Scheuer, M. Orenstein, J. Opt. Soc. Am. B 19 (2002) 732.
[13] F. Baronio, C. De Angelis, IEEE J. Quantum Electron. 38 (2002) 1309.
[14] I. Shadrivov, A. Zharov, J. Opt. Soc. Am. B 19 (2002) 596.
[15] Y. Kartashov, V. Vysloukh, L. Torner, Opt. Lett. 32 (2007) 2061.
[16] P. Dumais, A. Villeneuve, A. Saher-Helm, J.S. Aitchison, L. Friedrich, R.A. Fuerst, G.I. Stegeman, Opt. Lett. 25 (2000) 1282.
[17] L. Jankovic, H. Kim, G. Stegeman, S. Carrasco, L. Torner, M. Kats, Opt. Lett. 28 (2003) 2103.
[18] F. Baronio, C. De Angelis, P. Pioger, V. Couderc, A. Barthelemy, Opt. Lett. 29 (2004) 986.
[19] B. Alfassi, C. Rothschild, O. Manela, M. Segev, D. Christodoulides, Opt. Lett. 32 (2007) 154.
[20] M. Peccianti, G. Assanto, A. Dyadyusha, M. Kaczmarek, Opt. Lett. 32 (2007) 271.
[21] A. Alberucci, M. Peccianti, G. Assanto, Opt. Lett. 32 (2007) 2795.
[22] A. Barak, O. Peleg, C. Stucchio, A. Soffer, M. Segev, Phys. Rev. Lett. 100 (2008) 153901.
[23] U.K. Sapaev, G. Assanto, Opt. Express 17 (2009) 3765.
[24] M. Marangoni, D. Brida, M. Conforti, A. Capobianco, F. Baronio, G. Nalesso, C. De Angelis, R. Ramponi, G. Cerullo, Opt. Lett. 34 (2009) 241.
[25] F. Baronio, C. De Angelis, P. Pioger, V. Couderc, A. Barthelemy, Y. Min, V. Quiring, W. Sohler, Opt. Lett. 28 (2003) 2348.
[26] F. Baronio, C. De Angelis, M. Marangoni, C. Manzoni, R. Ramponi, G. Cerullo, Opt. Express 14 (2006) 4774.